Auto-calibration of Automotive MIMO Radars Using Simultaneous Localisation and Mapping

Petrov, Nikita; Yarovoy, Alexander

DOI
10.23919/EuRAD50154.2022.9784485

Publication date
2022

Document Version
Final published version

Published in
Proceedings of the 18th European Radar Conference

Auto-calibration of Automotive MIMO Radars Using Simultaneous Localisation and Mapping

Nikita Petrov[#1], Alexander Yarovoy[#2]
[#]Microwave Sensing, Signals and Systems (MS3)
Delft University of Technology
Mekelweg 4, 2628 CD, Delft, the Netherlands
{[1]N.Petrov, [2]A.Yarovoy}@tudelft.nl

***Abstract* — This paper presents a new method of automotive MIMO radar self-calibration which uses targets of opportunity embedded in road infrastructure, such as road signs and traffic lights. While conventional offline calibration of a phased array antenna requires accurate knowledge of the positions of calibration targets relative to the radar, such information is not available in a dynamic scenario. To compensate for this, we have developed an estimation procedure based on an extended Kalman filter (EKF) to address the challenge of simultaneous localisation, mapping and calibration. Numerical simulations demonstrate the possibility to decrease the sidelobes level and compensate the steering bias of a MIMO radar with the proposed method.**

***Keywords* — Radar, MIMO arrays, calibration, SLAM**

I. Introduction

The growing field of automotive radars operating in mm-waves (24 GHz, 77 GHz, 79 GHz bands) is highly interested in the development and maintenance of low-cost radars with high sensing performance. The current trend is to employ multiple-input, multiple-output (MIMO) radar systems, which combine instantaneous large-angle coverage with high accuracy, ac hived by applying high-resolution spectrum estimation techniques such as multiple signal decomposition (MUSIC). These techniques are very sensitive to calibration errors. Therefore, the proper calibration of MIMO arrays is vital to the performance of automotive radars. The presence of calibration errors degrade radar performance, particularly the accuracy and target response of (high-resolution) direction-of-arrival (DOA) estimation techniques [1], [2], interference cancellation and target detection.

Calibration of automotive radars has recently attracted widespread interest [3]. These techniques consider that the calibration is performed at the regular check of the auto, in a well controlled environment using corner reflectors installed at predefined locations [4] or more advanced systems form joint calibration of different type of sensors [5]. Various type of array imperfections (gain, phase, array element locations, mutual coupling between elements, I/Q imbalance) can be measured and compensated with a controlled calibration. However, it does not account for external factors such as temperature, humidity, aging, surface bend, etc. which can affect the performance of the radar between the regular checks. To tackle this problem auto-calibration is applied, which typically deals only a restricted class of errors, determined by a model with a finite number of unknown parameters [4].

Many auto-calibration methods developed to date are based either on an extension of the MUSIC algorithm [6] or on the maximum likelihood approach [7]. The key step in all of these techniques is estimating the signal covariance matrix, which requires the availability of a sufficient number of independent data samples (snapshots). It assumes a constant bearing of the measured targets over the observation time, yet this can hardly be satisfied with an automotive radar moving on the road. Non-negligible displacement of the car within the data collection time implies variation in the targets' angular locations and the smearing of the MUSIC spectrum. Moreover, the are developed for phased arrays calibration, and when applied to MIMO radars, they do not exploit fully exploit the structure of the data.

In this paper we propose a method for forward-looking automotive MIMO radar auto-calibration in operational mode. We focus on the estimation of the complex gains of antenna elements of MIMO arrays. This study is the extension of the study on phased array auto-calibration [8] to the case of MIMO radar. We use some principles of simultaneous localisation and mapping (SLAM) as a tool to extract the location of the sensor and the targets (hereinafter called landmarks) in the scene, necessary for proper array calibration. After formulating the problem of simultaneous localisation, mapping and calibration, we present an efficient solution for online sensor calibration in a dense target environment.

Notations: Hereinafter we use lowercase boldface letters for vectors, uppercase boldface letters for matrices, and uppercase boldface calligraphic letters for sets. The superscripts $(\cdot)^T$, $(\cdot)^H$ and $(\cdot)^*$ indicate matrix/vector transpose, Hermitian transpose and complex conjugate, respectively.

II. Problem statement

To develop the auto-calibration method, we expand the probabilistic formulation of the SLAM [9], [10] by including there sensor calibration. First, notice that the calibration of the phased array requires information about the (relative) sensor and targets (hereafter called landmarks) locations in order to form the expected target response [4]. In the general case of a platform moving in unknown environment,

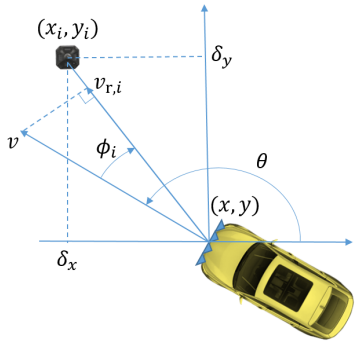

Fig. 1. Measurement geometry with one landmark at (x_i, y_i); $\phi_i < 0$

calibration problem can be written in a probabilistic way by: $P\left(\boldsymbol{\gamma}^{[t]}|\boldsymbol{\mathcal{Z}}^{[0:t]}, \boldsymbol{\mathcal{X}}^{[0:t]}, \mathbf{m}\right)$ which implies that in order to estimate the calibration vector $\boldsymbol{\gamma}^{[t]}$, the platform location[1] $\boldsymbol{\mathcal{X}}^{[0:t]} = \{\mathbf{x}^{[0]}, \ldots, \mathbf{x}^{[t]}\}$ and the map $\mathbf{m}$ should be known for every measurement $\boldsymbol{\mathcal{Z}}^{[0:t]} = \{\mathbf{z}^{[0]}, \ldots, \mathbf{z}^{[t]}\}$. This motivates the joint formulation of sensor auto-calibration with SLAM.

Combining the motivation above with the statistical definition of SLAM [9], we aim to estimate at each time step t the probability:

$$P\left(\mathbf{x}^{[t]}, \boldsymbol{\gamma}^{[t]}, \mathbf{m}|\boldsymbol{\mathcal{Z}}^{[0:t]}, \boldsymbol{\mathcal{U}}^{[0:t]}, \mathbf{x}^{[0]}\right), \tag{1}$$

which describes the problem of joint localisation – $\mathbf{x}^{[t]}$, calibration – $\boldsymbol{\gamma}^{[t]}$ and mapping – $\mathbf{m}$. This probability can be calculated via a recursive Bayesian filter, similarly to the original SLAM problem [9], [8]. The implementation of this Bayesian filter requires the definition on the observation (measurement) and dynamic (motion) models. The observation model $P(\mathbf{z}^{[t]}|\mathbf{x}^{[t]}, \boldsymbol{\gamma}^{[t]}, \mathbf{m})$ defines the probability of making the observation $\mathbf{z}^{[t]}$ for the given sensor and landmarks locations. The motion model $P(\mathbf{x}^{[t]}|\mathbf{x}^{[t-1]}, \mathbf{u}^{[t]})$ describes sensor motion in terms of the state transition with possible presence of control inputs $\boldsymbol{\mathcal{U}}^{[0:t]} = \{\mathbf{u}^{[0]}, \ldots, \mathbf{u}^{[t]}\}$. In this study we assume that the map is stationary and that the evolution of the calibration coefficients are defined by $P\left(\boldsymbol{\gamma}^{[t]}|\boldsymbol{\gamma}^{[t-1]}\right)$.

In this paper we focus on online filter-based SLAM, which estimates only the current position of the sensor (at time instant t only, rather than the whole trajectory) and it describes the map with a set of landmarks (targets). We demonstrate the applicability of continuous calibration with EKF SLAM. In general, calibration can be incorporated in other types of feature-based SLAM in a similar manner.

III. Data model

The state vector contains the sensor and landmarks parameters, essential to define the observation model, which can be grouped into three parts: $\mathbf{s}^{[t]} = [\mathbf{x}^{[t]}, \boldsymbol{\gamma}^{[t]}, \mathbf{m}_1, \ldots, \mathbf{m}_I]^T$. For the localization in a plane, the vehicle location (x, y), orientation θ and instantaneous velocity v form the state subvector $\mathbf{x}^{[t]} = [x, y, \theta, v]^T$[2].

[1]It is assumed that the platform location corresponds to the radar location.
[2]To simplify the notations we skipped the time index for scalar variables.

The calibration coefficients are represented by their real and imaginary parts the calibration $\boldsymbol{\gamma}^{[t]} = [\gamma_1^R, \ldots, \gamma_{K-1}^R, \breve{\gamma}_1^R, \ldots, \breve{\gamma}_{L-1}^R, \gamma_1^I, \ldots, \gamma_{K-1}^I, \breve{\gamma}_1^I, \ldots, \breve{\gamma}_{L-1}^I]^T \in \mathbb{R}^{2(K+L-2)\times 1}$, essential for the estimation routing. Finally, the map, assumed stationary, consists of I point-like landmarks with Cartesian locations $\mathbf{m}_i = [x_i, y_i]^T, i = 1, \ldots, I$.

A. MIMO array response

Consider a coherent MIMO radar with K transmit (Tx) and L receive (Tx) channels arranged in uniform linear arrays (ULA), which observes a point-like target at angle ϕ_i from the array pointing direction, see Fig. (1). The target is characterised by its complex back-scattering coefficient $\alpha_i = |\alpha_i|e^{j\varphi_i}$ with $\varphi_i \sim \mathcal{U}(0, 2\pi)$, which comprises signal attenuation due to two-way propagation and processing gain with no loss of generality. The amplitude and phase distortion in the k-th transmit element is characterised by a complex-valued coefficient γ_k, $k = 0, \ldots, K-1$ and in the l-th receive element by $\breve{\gamma}_l$, $l = 0, \ldots, L-1$. Then, the response of the i-th target associated with the k-th transmit and l-th receive channel is given by:

$$\kappa_{k,l,i} = \alpha_i \gamma_k \breve{\gamma}_l \exp\left(\psi_{k,l,i}\right) + n_{k,l,i}, \tag{2}$$

where

$$\psi_{k,l,i} = -j2\pi \frac{d_t k + d_r l}{\lambda} \sin(\phi_i), \tag{3}$$

λ stands for the carrier wavelength, d_t and d_r are the inter-element spacing of the Tx and Rx arrays and $n'_{k,l,i} \sim \left(0, \sigma_n^2\right)$ represents the receiver noise. To remedy the dependence on the target back-scattering coefficient α_i, we consider channel $k = 0, l = 0$ (another k and l can be used with no loss of generality) as the reference point and remove it from the measurements after normalization. This implies that the calibration coefficients $\gamma_0 = 1$ and $\breve{\gamma}_0 = 1$ are fixed and $KL - 1$ normalized measurements are:

$$p_{k,l,i} = \frac{\kappa_{k,l,i}}{\kappa_{0,0,i}} = \gamma_k \breve{\gamma}_l \exp\left(\psi_{k,l,i}\right) + n'_{k,l,i}, \tag{4}$$

$k = 0, \ldots, K-1$, $l = 0, \ldots, L-1$, $(k + l) \geq 1$. The noise after normalization is $n'_{k,l,i} \sim \left(0, \sigma_i^2\right)$ becomes a function of landmark SNR: $\sigma_i^2 = \left(|\alpha_i|^2/\sigma_n^2 + 1\right)^{-1} = (\mathrm{SNR}_i + 1)^{-1}$.

B. Observation model

Consider the geometry presented in Fig. 1. At time t the radar observes N landmarks: $\mathbf{z}^{[t]} = [\mathbf{z}_{i_1}^T, \ldots, \mathbf{z}_{i_N}^T]^T$ with indexes $\{i_1, \ldots, i_N\}$ in the global map. We assume that the data association problem is correctly resolved. The observation vector of a point-like target consist of the measured range, radial velocity (we assume that no velocity ambiguities occurs) and the normalized response of the MIMO array $\mathbf{z}_i = [r_i, v_{r,i}, p_{0,1,i}^R, \ldots, p_{K-1,L-1,i}^R, p_{0,1,i}^I, \ldots, p_{K-1,L-1,i}^I]^T \in \mathbb{R}^{2M\times 1}$. Similarly to the calibration coefficients, the complex responses in MIMO channels are represented by their real and imaginary parts. To simplify the notations, define an auxiliary variable

$$\phi_i = \mathrm{atan2}\left(y_i - y, x_i - x\right) - \theta. \tag{5}$$

where $\mathrm{atan2}\,(y,x)$ evaluates the angle of the vector in the Euclidean plane, given its coordinates (x,y). Then the measurement of the i-th target at time t defines the observation model:

$$\begin{aligned} r_i &= \sqrt{(x_i-x)^2+(y_i-y)^2}; \\ v_{\mathrm{r},i} &= v\cos(\phi_i); \\ p^R_{k,l,i} &= a_1\cos(\psi_{k,l,i}) - a_2\sin(\psi_{k,l,i}); \\ p^I_{k,l,i} &= a_1\sin(\psi_{k,l,i}) + a_2\cos(\psi_{k,l,i}); \end{aligned} \tag{6}$$

where $\psi_{k,l,i}$ was defined in (3) and

$$\begin{bmatrix} a_1 & a_2 \end{bmatrix} = \begin{bmatrix} \gamma^R_k\breve{\gamma}^R_l - \gamma^I_k\breve{\gamma}^I_l & \gamma^R_k\breve{\gamma}^I_l + \gamma^I_k\breve{\gamma}^R_l \end{bmatrix}. \tag{7}$$

The observation model (6) can be seen as a nonlinear function of multiple variables $\mathbf{g}^{[t]}_i\left(\mathbf{s}^{[t]}_i\right)$ in the EKF. The corresponding Jacobian for the i-th target measurement $\mathbf{G}^{[t]}_i \in \mathbb{R}^{2KL\times 2(K+L+1)}$ has a block structure:

$$\mathbf{G}^{[t]}_i = \left.\frac{\partial \mathbf{g}^{[t]}_i}{\partial \mathbf{s}^{[t]}_i}\right|_{\mathbf{s}^{[t]}_i=\bar{\mathbf{s}}^{[t]}_i} = \begin{bmatrix} \mathbf{G}_{\mathrm{rv,x}} & \mathbf{G}_{\mathrm{rv},\gamma} & \mathbf{G}_{\mathrm{rv,m}} \\ \mathbf{G}_{\mathrm{ar,x}} & \mathbf{G}_{\mathrm{ar},\gamma} & \mathbf{G}_{\mathrm{ar,m}} \end{bmatrix}, \tag{8}$$

where we have skipped target i and time t indices of submatrices. The first notation in subscript – rv and ar – defines the set of measurement equations from (6) to which the Jacobian is calculated: rv corresponds to range and velocity measurements, while ar refers to the MIMO array measurements. The second notation indicates the relevant part of the state vector: the sensor location $\mathbf{x}=[x,y,\theta,v]^T$ — x, the calibration coefficients $\boldsymbol{\gamma}$ — γ or the i-th landmark location $\mathbf{m}_i=[x_i,y_i]^T$ — m. The partial derivatives of $[r_i, v_{\mathrm{r},i}]^T$ in (6) over $\mathbf{x}$ gives sumbatrix $\mathbf{G}_{\mathrm{rv,x}} \in \mathbb{R}^{2\times 4}$:

$$\mathbf{G}_{\mathrm{rv,x}} = \frac{1}{q}\begin{bmatrix} -\sqrt{q}\delta_x & -\sqrt{q}\delta_y & 0 & 0 \\ -v\sin(\phi_i)\delta_y & v\sin(\phi_i)\delta_x & v\sin(\phi_i)q & \cos(\phi_i). \end{bmatrix}, \tag{9}$$

where $\delta_x = x_i - x$, $\delta_y = y_i - y$ and $q=(x_i-x)^2+(y_i-y)^2$. Range and velocity measurements do not depend on the MIMO calibration, thus $\mathbf{G}_{\mathrm{rv},\gamma} = \mathbf{0}_{2\times 2(K+L-2)}$. Finally, $\mathbf{G}_{\mathrm{rv,m}} \in \mathbb{R}^{2\times 2}$ relates range/velocity measurements to the landmark location via:

$$\mathbf{G}_{\mathrm{rv,m}} = \frac{1}{q}\begin{bmatrix} \sqrt{q}\delta_x & \sqrt{q}\delta_y \\ v\sin(\phi_i)\delta_y & -v\sin(\phi_i)\delta_x \end{bmatrix}. \tag{10}$$

The submatrices of the Jacobian (8) which correspond to the array measurements (6) can be given in a compact form by noticing that location- and landmark-related state variables contribute to the array response $p^R_{k,l,i}, p^I_{k,l,i}$ only via $\psi_{k,l,i}$, see (3), (5), (6). This leads to the expressions:

$$\begin{aligned} \frac{\partial p^R_{k,l,i}}{\partial \xi} &= \left(-a_1\sin(\psi_{k,l,i}) + a_2\cos(\psi_{k,l,i})\right)\frac{\partial \psi_{k,l,i}}{\partial \xi}; \\ \frac{\partial p^I_{k,l,i}}{\partial \xi} &= \left(a_1\cos(\psi_{m,i}) - a_2\sin(\psi_{k,l,i})\right)\frac{\partial \psi_{k,l,i}}{\partial \xi}, \end{aligned} \tag{11}$$

valid for the platform location- and landmark-related variables of the state vector: $\xi \in \{\mathbf{x}, \mathbf{m}_i\} = \{x, y, \theta, v, x_i, y_i\}$. The partial derivative of $\psi_{k,l,i}$ over the platform location variables $\mathbf{x}$ gives 1×4 vector:

$$\frac{\partial \psi_{k,l,i}}{\partial \mathbf{x}} = -2\pi m\frac{d}{\lambda}\cos(\psi_{k,l,i})\frac{1}{q}\begin{bmatrix} \delta_y & -\delta_x & -q & 0 \end{bmatrix}. \tag{12}$$

Finally, the block of Jacobian $\mathbf{G}_{\mathrm{ar,x}} \in \mathbb{R}^{2(KL-1)\times 4}$ is built by stacking $KL-1$ rows of (11) for real measurements in channels $k=0,\ldots,K-1$, $l=0,\ldots,L-1$, $(k+l)\geq 1$ and their counterparts for the imaginary data.

Next, we find the partial derivative of $\psi_{k,l,i}$ over the landmark variables $\mathbf{m}_i$:

$$\frac{\partial \psi_{k,l,i}}{\partial \mathbf{m}_i} = -2\pi m\frac{d}{\lambda}\cos\psi_{k,l,i}\frac{1}{q}\begin{bmatrix} -\delta_y & \delta_x \end{bmatrix} \tag{13}$$

and concatenate the rows related to real and imaginary measurements of all channels in the similar order as above to form $\mathbf{G}_{\mathrm{ar,m}} \in \mathbb{R}^{2(KL-1)\times 2}$.

The last block $\mathbf{G}_{\mathrm{ar},\gamma} \in \mathbb{R}^{2(KL-1)\times 2(K+L-2)}$ of the Jacobian (8) corresponds to the partial derivatives of the MIMO measurements $p^R_{k,l,i}, p^I_{k,l,i}$ with respect to the calibration coefficients $\gamma_k, \breve{\gamma}_l$. The measurement in each transmit-receive pair depends only on two calibration coefficients in these channels and thus the submatrix $\mathbf{G}_{\mathrm{ar},\gamma}$ is sparse. The derivatives can be calculated directly from (6), (8).

Finally, all of the measurements at time t associated with the targets form the vector $\mathbf{z}^{[t]}$, and the corresponding Jacobian matrix $\mathbf{G}^{[t]}$ is built [10]. The noise for every measurement is defined by its real and imaginary parts and from (4) it follows $\omega_i \sim (0, \sigma^2_{p,i})$, where $\sigma^2_{p,i} = \frac{\sigma^2_n}{2\left(\alpha^2_i+\sigma^2_n\right)}$. Together with errors in range and Doppler measurements, it forms $\boldsymbol{\omega} \sim \mathcal{N}(0, \mathbf{R})$, where $\mathbf{R_i} = \mathrm{diag}\left(\sigma^2_r, \sigma^2_{vr}, \sigma^2_{p,i}\mathbf{1}_{1\times 2(KL-1)}\right)$.

C. Dynamic model

The dynamic model describes the movement of the platform and landmarks in time: $\mathbf{s}^{[t]} = \mathbf{a}^{[t]}\left(\mathbf{s}^{[t-1]}\right) + \mathbf{u}^{[t]}$. The landmarks are assumed stationary – the common assumption in SLAM [10]. The platform moves with a nearly constant velocity model:

$$\begin{aligned} x^{[t]} &= x^{[t-1]} + Tv^{[t-1]}\cos(\theta^{[t-1]}); \\ y^{[t]} &= y^{[t-1]} + Tv^{[t-1]}\sin(\theta^{[t-1]}); \\ \theta^{[t]} &= \theta^{[t-1]} + u^{[t]}_\theta; \\ v^{[t]} &= v^{[t-1]} + u^{[t]}_v, \end{aligned} \tag{14}$$

where T is the time interval between the measurements and $u^{[t]}_\theta \sim \mathcal{N}(0,\sigma^2_\theta)$ and $u^{[t]}_v \sim \mathcal{N}(0,\sigma^2_v)$ define the driving noise of bearing and velocity. Time variation of real and imaginary parts of the calibration coefficients in both Tx and Rx channels are modeled by: $\gamma^{\{R,I\},[t]}_{\{k,l\}} = \gamma^{\{R,I\},[t-1]}_{\{k,l\}} + w^{\{R,I\},[t]}_m$, where $w^R_{m,t}, w^I_m \sim \mathcal{N}\left(0,\sigma^2_w\right)$ and $\sigma_w \in [10^{-6}, 10^{-3}]$.

Every measurement is then associated with an existing landmark, or a new landmark is created. All of the measurements associated with existing landmarks form the measurement vector $\mathbf{z}^{[t]}$, and the Jacobian matrix $\mathbf{G}^{[t]}$ is built from the corresponding blocks $\mathbf{G}^{[t]}_i$ (8) as e.g. in [10]. After this data arrangement a standard EKF can be applied.

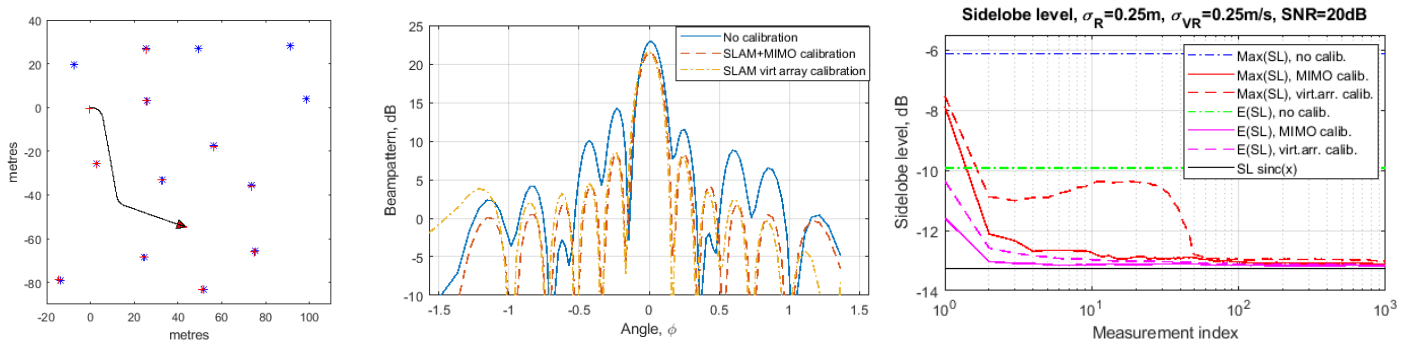

a *b* *c*

Fig. 2. (*a*) Estimated trajectory with the true (blue) and estimated (red) map, (*b*) Array response before and after auto-calibration, (*c*) Peak-to-sidelobe level vs number of scans.

IV. Simulations

To demonstrate the proposed approach we modified the EKF-SLAM simulator created by Tim Bailey [11]. We consider a MIMO radar operating at the frequency $f_c = 77$ GHz with a dense Rx array of $L = 4$ elements and sparse Tx array with $K = 3$ and $d_t = 2\lambda$. The calibration errors are modeled as $\gamma_k^R, \breve{\gamma}_l^R \sim \mathcal{N}(1, \sigma_\gamma^2)$ and $\gamma_k^I, \breve{\gamma}_l^I \sim \mathcal{N}(0, \sigma_\gamma^2)$, with $\sigma_\gamma = 0.2$. SNR of all measurements is 20 dB, independently on the range to the target.

The observation area of the radar is limited in range by $R \leq R_{\max} = 50$ m and in angle by $|\phi| \leq \phi_{\max} = 75^o$. The platform moves with constant velocity $v_0 = 3$ m/s, and its control inputs have Gaussian error in velocity and heading with $\sigma_v = 0.3$ m/s and $\sigma_\theta = 3^o$, respectively. The dynamic noise of the calibration coefficients is set to $\sigma_w = 10^{-5}$.

The simulated map is shown in Fig. 2, *a* in blue with the trajectory of the vehicle and estimated map (in red). The antenna pattern of uncalibrated array and its counterpart at the end of the trajectory using the proposed approach and virtual array calibration [8] are shown in Fig. 2, *b*. Both calibration technique recovers the sinc-like pattern of a calibrated array with a minor difference between them. The difference in the maximum response on the array is due usage of the constrain $\gamma_0 = 1$ and $\breve{\gamma}_0 = 1$ rather than the norm of the calibration vector. Further, we compare the performance of the auto-calibration by evaluating the sidelobe level over 100 Monte-Carlo trials of the trajectory shown in Fig. 2, *a*. The average (E) and the maximum over realizations peak sidelobe level (PSL) as the function of number of measurements are shown in Fig. 2, *c*. We noticed that for small to moderate calibration errors (here $\sigma_\gamma = 0.2$) MIMO calibration converges faster to the steady state compared to the full virtual array calibration. With about 50 measurements, both techniques converge to PSL ≈ -13 dB of a well-calibrated array.

V. Conclusion

In this paper we have proposed a novel technique for forward-looking MIMO radar auto-calibration under operational conditions. It was shown that the dynamic calibration of automotive radar using targets of opportunity can be realized jointly with sensor localisation and mapping. The proposed MIMO auto-calibration converges faster to the steady state compared to the full virtual array auto-calibration in presence of small to moderate calibration errors.

Acknowledgements

This work is supported in part by NWO TTW under the project STW #13563: “Standardized Self-Diagnostic Sensing Systems for Highly Automated Driving”.

References

[1] K. Carver, W. Cooper, and W. Stutzman, “Beam-pointing errors of planar phased arrays,” *IEEE Transactions on Antennas and Propagation*, vol. 21, no. 2, pp. 199–202, 1973.

[2] B. Porat and B. Friedlander, “Accuracy requirements in off-line array calibration,” *IEEE transactions on aerospace and electronic systems*, vol. 33, no. 2, pp. 545–556, 1997.

[3] M. Harter, J. Hildebrandt, A. Ziroff, and T. Zwick, “Self-calibration of a 3-D-digital beamforming radar system for automotive applications with installation behind automotive covers,” *IEEE Transactions on Microwave Theory and Techniques*, vol. 64, no. 9, pp. 2994–3000, 2016.

[4] M. Viberg, M. Lanne, and A. Lundgren, “Calibration in array processing,” in *Classical and Modern Direction-of-Arrival Estimation*. Elsevier, 2009, pp. 93–124.

[5] J. Domhof, R. Happee, and P. Jonker, “Multi-sensor object tracking performance limits by the cramer-rao lower bound,” in *2017 20th International Conference on Information Fusion (Fusion)*. IEEE, 2017, pp. 1–8.

[6] A. J. Weiss and B. Friedlander, “Eigenstructure methods for direction finding with sensor gain and phase uncertainties,” *Circuits, Systems and Signal Processing*, vol. 9, no. 3, pp. 271–300, 1990.

[7] B. C. Ng and C. M. S. See, “Sensor-array calibration using a maximum-likelihood approach,” *IEEE Transactions on Antennas and Propagation*, vol. 44, no. 6, pp. 827–835, 1996.

[8] N. Petrov, O. Krasnov, and A. Yarovoy, “Auto-calibration of automotive radars in operational mode using simultaneous localisation and mapping,” *IEEE Transactions on Vehicular Technology*, 2021.

[9] H. Durrant-Whyte and T. Bailey, “Simultaneous localization and mapping: part I,” *IEEE robotics & automation magazine*, vol. 13, no. 2, pp. 99–110, 2006.

[10] S. Thrun, W. Burgard, and D. Fox, *Probabilistic robotics*. MIT press Cambridge, 2000, vol. 1.

[11] T. Bailey, “SLAM package of Tim Bailey.” [Online]. Available: https://openslam-org.github.io/bailey-slam.html